# Title

## Design and First-Principles Calculation of Pt-Doped Phenalene Basket for Enhanced Photocatalytic Hydrogen Evolution: Structural, Optical, and Electronic Insights

**Author: Chukwu, Chidi Daniel**

**Affiliation: University of Electronic Science and Technology of China**

# Abstract

Charge recombination represents a significant challenge to progress in the field of photocatalytic hydrogen evolution reaction. In this study, we present our findings on the design and first-principle calculation of a proposed efficient photocatalytic basket material with the potential to significantly enhance photocatalytic hydrogen evolution. The modeling of the design was executed using Chemdraw, while the optimization, optical and electronic property calculation, and adsorption property calculation were conducted utilizing DMOL$^3$ and Adsorption Locator. Confirmation of the structure's platinum content was obtained through the reassignment of bond characteristics previously observed between $C_4$-$C_5$, $C_5$-$C_6$, and $C_5$-$C_{10}$. These bonds were redefined to reflect interactions involving platinum, specifically $Pt_4$-$C_5$, Pt4-$C_7$, and $Pt_4$-$C_3$. The bond angles $Pt_4$-$C_3$-$C_2$ (120.625°) and $Pt_4$-$C_5$-$C_{10}$ (120.624°) were not present in the original phenalene structure. The absorption peak of 0.0223 nm and 0.005 nm for Pt-doped phenalene provide critical insights into its optical properties, underscoring its potential for advanced photonic applications. The HOMO-LUMO energy difference for platinum-doped phenalene ranges from -0.409 eV to -0.285 eV. The Mulliken electrophilic indices reveal that platinum in the Pt-doped phenalene carries a partial positive charge of 0.101eV, whereas the bonding carbons ($C_3$, $C_5$, and $C_7$) have much smaller partial charges of 0.017eV. The observed Gibbs free energy values for $H_2$ (-0.24157 eV) and $H^+$ (-0.11589 eV) are further confirmed. This study's findings highlight the Pt-doped phenalenes' excellent performance and stability as catalysts. Its optical and electronic properties make it a contender in photocatalytic energy conversion and environmental remediation, propelling sustainable hydrogen production.

**Keywords: Phenalene, HER, Charge Recombination, Photocatalysis, SAC, Optics, Organic Photocatalist basket**

# 1.0 Introduction

Photocatalytic hydrogen evolution (HER) has garnered significant attention in recent years as a promising method for sustainable hydrogen production. Among the various strategies employed, single-atom photocatalysis stands out as an innovative approach [1]. In single-atom photocatalysis, metal atoms are isolated and anchored on a support material, allowing for the maximum exposure of active sites [2]. This unique configuration facilitates highly efficient light absorption and electron transfer, making single-atom photocatalysts (SACs) particularly valuable in the HER process. Their ability to function effectively under ambient conditions, coupled with the possibility of tuning their electronic properties through careful material design, has positioned SACs as a critical component in advancing hydrogen production technologies [3]. Their importance lies in the potential for high catalytic efficiency with low loading of precious metals, thus reducing the overall cost of photocatalytic systems.

Organic photocatalysis has emerged as a versatile and cost-effective alternative to traditional inorganic photocatalysts in the field of HER [4]. Organic photocatalysts, particularly small organic molecules and conjugated polymers, are attractive due to their tunable electronic properties, which can be engineered to match the light absorption spectra of the solar spectrum [5]. The presence of conjugated π-electrons in organic materials facilitates efficient electron transfer upon light excitation, making them suitable for catalyzing the hydrogen evolution reaction [6]. Moreover, organic photocatalysts are often light, flexible, and capable of being processed into thin films or coatings, offering additional advantages in terms of scalability and ease of integration into renewable energy systems [7]. This flexibility, combined with their generally lower toxicity compared to metal-based catalysts, makes organic photocatalysts an appealing choice for large-scale HER applications.

The properties [8] of organic photocatalysts play a crucial role in their effectiveness for HER. The absorption of visible light, due to their narrow bandgaps, allows organic materials to utilize a broader spectrum of sunlight, increasing their potential efficiency. Additionally, low-cost synthesis methods, along with the ability to modify their structure at the molecular level, enable fine-tuning of their electronic properties for enhanced photocatalytic activity [9]. The charge carrier dynamics, such as efficient charge separation and transfer, are optimized through the careful design of organic materials, allowing for better hydrogen production rates [10]. Furthermore, heteroatom doping, such as introducing nitrogen or sulfur into the organic structure, has been shown to significantly improve the electronic properties and the stability of the photocatalysts, enabling long-term hydrogen evolution without significant degradation [11].

Despite their promising properties, organic photocatalysts face several challenges that hinder their efficiency in HER [12-15]. One major issue is the low stability of many organic materials under harsh photocatalytic conditions, particularly in aqueous environments [16]. These materials are susceptible to photocorrosion, which can reduce their lifetime and effectiveness over time. Additionally, while organic photocatalysts are capable of absorbing sunlight efficiently, poor charge separation often occurs due to the relatively low conductivity of many organic materials. This leads to the rapid recombination of photogenerated charge carriers, which reduces the overall efficiency of the HER process [17-19]. The recombination of electrons before they can participate in the hydrogen evolution reaction results in a significant loss of available energy, making it one

of the most critical challenges to overcome for enhancing the performance of organic photocatalysts in HER.

The phenomenon of electron recombination is particularly detrimental to photocatalytic hydrogen evolution efficiency. When a photocatalyst absorbs light, it generates electron-hole pairs [20]; however, if these charge carriers recombine before they can be utilized in the HER process, the catalytic efficiency is significantly reduced. Electron recombination occurs when the excited electrons and holes return to their original states, releasing energy in the form of heat or light instead of driving the desired reaction. In organic photocatalysts, poor charge separation and slow electron transfer rates exacerbate this issue [21-23]. Additionally, the lack of efficient electron transport networks in organic materials can hinder the migration of charge carriers to the catalytic sites, increasing the likelihood of recombination. Tackling this challenge requires the development of advanced materials that can not only promote effective charge separation but also facilitate rapid charge transport to the reaction sites, thereby improving the efficiency of HER processes.

Here, we present the findings of an efficient HER photocatalytic model with limited electron recombination and stable, comparable optical properties. The model demonstrates a robust ability to maintain long-term catalytic activity, even under harsh reaction conditions, by minimizing charge carrier loss and enhancing charge separation efficiency. Furthermore, it is expected that the photocatalyst would exhibit excellent light absorption across a wide spectrum, ensuring optimal utilization while maintaining structural integrity throughout the hydrogen evolution process. This anticipated combination of high efficiency and stability positions the model as a promising candidate for scalable, sustainable hydrogen production.

## 2.0 Physical properties of Phenalene

Phenalene [24] is noteworthy for its propensity to generate stable anions, cations, and radicals. Quantum mechanical analyses have demonstrated that the anion, cation, and radical of phenalene possess equivalent π-electron delocalization energies [25-27]. The properties have been studied and reported to exhibit remarkable physical properties. Notably, phenalene has been observed to generate a relatively stable anion, cation, and radical [28]. Quantum mechanical studies have provided a satisfactory explanation for the observed stability of these molecules. A comprehensive report on the structural properties noted that the bond distances and their changes in the naphthalene-like fragment are similar to those of phenalene. However, changes in the C-C bond distances involving sp3-hybridized carbon atoms exhibit significant variation depending on the specific location of hydrogen addition. The disruption of aromaticity leads to the elongation of C1−C9 (1.52 Å) and $C_1$−$C_2$ bonds (1.50 Å), both of which correspond to a single C−C bond. This disruption also results in the localization of single and double bonds to $C_3$−$C_3$ (1.47 Å) and $C_2$−$C_3$ (1.34 Å), respectively. Furthermore, a variant with the elongation of the bonds connecting the sp3-hybridized $C_2$ is analogous (1.47 Å for $C_2$−$C_1$ and $C_2$−$C_3$), while $C_1$−$C_{9a}$ and $C_3$−$C_{3a}$ correspond to aromatic bonds with distances of 1.40 Å [29].

### 2.1 Electrical Properties of Phenalene

Phenalene displays distinctive electrical characteristics attributable to its intrinsic structure, which is distinguished by a delocalized π-electron system [30, 31]. This property renders it a promising candidate

for applications in organic electronics. It readily forms stable anions, cations, and radicals, with the negative charge predominantly localized on the central carbon atom in its anionic form. This property signifies its capacity to readily accept electrons and potentially conduct electricity when appropriately doped or modified. The next paragraphs will dwell more on the attractive properties of phenalene.

*High Electron Affinity* [32]*:* The delocalized π-electron system in phenalene allows it to efficiently accept electrons, making it an excellent electron acceptor molecule with potential applications in electronic and optoelectronic devices.

*Radical stability* [33]*:* Phenalene can form a remarkably stable radical species due to its aromatic π-system, which effectively delocalizes unpaired electrons. This stability enhances its role in charge transport mechanisms and makes it a promising candidate for organic semiconductors and redox-active materials.

*Potential for conductivity:* While phenalene is not inherently highly conductive, reports has pointed out its potential for conductivity [34]. Its electrical properties can be significantly improved through chemical doping. Introducing suitable dopants can inject additional electrons or holes into the system, creating charge carriers that enable high conductivity. This tunability makes phenalene a versatile material for use in organic electronic devices.

*π-conjugation:* The extensive π-conjugation [35] across the phenalene molecule facilitates efficient electron delocalization, reducing energy loss and enhancing charge mobility. This property is crucial for its performance in conductive applications, as it allows for seamless charge transport over long molecular distances, contributing to its potential as a material for next-generation electronic and energy devices."

## 2.2 Optical Properties of Phenalene

Phenalene demonstrates a high degree of absorption in the visible light spectrum due to its conjugated pi-electron system, resulting in a distinctive deep red coloration [36]. Its optical properties are predominantly characterized by its propensity to readily form a stable radical anion (phenalenyl radical) with a delocalized negative charge on the central carbon atom. This radical anion exerts a substantial influence on the absorption and emission characteristics of the phenalene. From the optical perspective, the attractive properties are given below.

*Intense color:* Phenalene exhibits a striking deep red hue due to its strong absorption in the visible region, particularly at longer wavelengths [37-40]. This vivid coloration is a result of its extensively conjugated π-electron system, which lowers the energy gap between the HOMO and LUMO, allowing efficient absorption of visible light and contributing to its optical richness.

*Radical anion formation:* A defining characteristic of phenalene is its remarkable ability to readily form a stable phenalenyl radical anion [41-43]. This stability arises from the delocalization of unpaired electrons over the conjugated system, making the radical anion a key player in the unique electronic and optical properties of phenalene. Such radical species have potential applications in charge transport and redox-active systems.

*Absorption spectra:* The absorption spectrum of phenalene is characterized by a broad band in the visible region, with a peak typically in the range of **500-600 nm** [44-46], depending on environmental factors such as the solvent, pH, and specific substituents. This broad and intense absorption makes phenalene and its derivatives attractive for optoelectronic and light-harvesting applications.

*Fluorescence:* While pristine phenalene may exhibit weak fluorescence due to non-radiative decay pathways, its derivatives, particularly those with strategically positioned electron-donating [47, 48] or electron-withdrawing groups, can demonstrate strong and tunable fluorescence. These derivatives emit light across a range of wavelengths, depending on the substituents and their electronic effects, making them useful in sensing, imaging, and light-emitting applications.

*Electrochromism:* Phenalene's ability to easily form a radical anion under applied potential gives it notable electrochromic behavior [49]. This means that its color can shift dramatically upon electrical stimulation, driven by changes in its electronic structure. This property, combined with its stability and optical tunability, positions phenalene as a promising material for **electrochromic devices**, such as smart windows, display panels, and adaptive camouflage technologies.

## 2.3 Platinum Excellent Catalytic Prowess

Platinum is widely recognized as an outstanding catalyst for the Hydrogen Evolution Reaction (HER) due to its unparalleled catalytic properties [50, 51]. Its optimal hydrogen binding energy ensures efficient hydrogen adsorption and desorption, enabling high-performance hydrogen production with minimal overpotential. This makes platinum one of the most active and reliable catalysts for HER. However, its high cost and scarcity pose significant challenges, limiting its large-scale application and driving the search for alternative, cost-effective materials.

Platinum possess excellent properties that makes it most suitable for HER and most are itemized below.

*High catalytic activity:* Platinum exhibits exceptional catalytic activity for HER, outperforming most other materials [52]. This is evidenced by its ability to achieve high current densities at very low overpotentials, ensuring energy-efficient hydrogen production.
*Optimal hydrogen binding energy:* The remarkable HER performance of platinum is attributed to its ideal hydrogen adsorption energy. It strikes a perfect balance between binding [53] hydrogen atoms strongly enough to enable efficient electron transfer while ensuring easy desorption of hydrogen gas, a critical step for sustained catalytic performance.
*Versatility in different environments:* Platinum is highly adaptable, functioning effectively as a catalyst in both acidic and alkaline media. This versatility [54, 55] allows its use across a wide range of HER systems, including those integrated into electrolyzers, fuel cells, and renewable energy technologies.

These qualities underscore platinum's significance as a benchmark HER catalyst, but its limitations in cost and availability continue to motivate ongoing research into alternative materials with comparable activity and greater sustainability. A single atom photocatalyst born of these two has the potential of pushing boundaries for hydrogen evolution without charge recombination barriers.

# 3.0 Computational Approach

## 3.1 Gradient Descent assisted geometry optimization

DMol³ was used to calculate the geometry optimization of the system, employing the gradient descent method as the primary algorithm for minimizing the total energy of the system [56]. Geometry optimization aims to find the equilibrium configuration of a molecular or solid-state system, where the total potential energy is minimized, and the forces on all atoms approach zero. The gradient descent method iteratively updates the atomic positions along the direction of the steepest descent of the energy gradient. Mathematically, the position of an atom at step $n^{+1}$ is updated based on the gradient of the potential energy E with respect to its coordinates, expressed as in equation (**1**):

$$Rn+1=Rn-\alpha\nabla E \quad (1)$$

where Rn is the position vector at step n
α is the step size,
∇E is the gradient of the energy with respect to the atomic positions.

This approach ensures a progressive reduction in energy at each iteration, guiding the system towards its lowest energy configuration.

In the gradient descent method, convergence is achieved when the magnitude of the forces, **|∇E|**, falls below a predefined threshold, indicating that the atoms are near their equilibrium positions. To improve convergence efficiency, advanced implementations often include dynamic adjustments of the step size α to balance between stability and rapid convergence [57]. For systems with many degrees of freedom, the potential energy surface (**PES**) can exhibit local minima, and the algorithm is designed to avoid being trapped in these through careful initialization and adaptive corrections. The total potential energy is evaluated using density functional theory **(DFT)**, and the forces (**equation 2**) are derived as the negative gradient of this energy,

$$F=-\nabla E. \quad (2)$$

The iterative process in DMol³ continues until both the energy and the atomic forces meet the convergence criteria, ensuring the optimized geometry corresponds to a physically meaningful and energetically favorable configuration.

## 3.2 Van der waals and Electrostatic calculation of the Rigid adsorption Energy

The Adsorption Locator in Materials Studio [58, 59] calculates the rigid adsorption energy to evaluate how molecules interact with surfaces without considering structural relaxations. The rigid adsorption energy (**equation 3**), is defined as the energy difference between the total energy of the combined adsorbate-surface system and the sum of the energies of the isolated surface and adsorbate. This is expressed as:

$$E_{ads}^{Rigids} = E_{total} - (E_{surface} + E_{adsorbate}) \quad (3)$$

Here, $E_{total}$ is the total energy of the system with the adsorbate in a fixed geometry on the surface, while $E_{surface}$ and $E_{adsorbate}$ are the energies of the isolated surface and adsorbate, respectively. This calculation enables an assessment of adsorption strength and interaction energy without altering the atomic positions.

To account for van der Waals **(vdW)** interactions [60], the Adsorption Locator employs dispersion-corrected methods or force-field approximations. The vdW energy (**equation 4**) is typically modeled using the Lennard-Jones potential:

$$E_{vDW} = 4_{\varepsilon} \left[\left(\frac{\sigma}{r}\right)^{12} - \left(\frac{\sigma}{r}\right)^{6}\right] \quad (4)$$

where r is the interatomic distance, ε represents the potential well depth, and σ is the distance at which the potential energy is zero.

This equation captures the balance between attractive and repulsive vdW forces, which are crucial for describing weak adsorption and physisorption phenomena. Incorporating vdW forces provides a detailed picture of non-covalent interactions between the adsorbate and surface.

## 3.3 MATLAB assisted Overpotential Calculation

Using the MATLAB console to calculate overpotential is highly convenient due to its robust computational capabilities and ease of handling complex equations. MATLAB provides built-in functions for solving electrochemical models, plotting current-voltage curves, and performing numerical optimization, making it ideal for analyzing overpotential. Its interactive environment allows for quick parameter adjustments and real-time visualization of results, streamlining the iterative process of evaluating and optimizing electrochemical systems.

The code adopted for calculating the HER overpotential is given below;

```
% Given Gibbs free energies (in eV)
G_H = -0.11589;  % Gibbs free energy for proton (H+)
G_H2 = -0.24157;  % Gibbs free energy for hydrogen molecule (H2)

% Thermoneutral Gibbs free energy (ideal, assumed to be 0 eV)
G_thermoneutral = 0;

% Calculate the overpotential for HER
overpotential_H = G_H - G_thermoneutral;  % Overpotential for proton adsorption
overpotential_H2 = G_H2 - G_thermoneutral; % Overpotential for hydrogen desorption

% Display results
disp(['Overpotential for H+ adsorption: ', num2str(overpotential_H), ' eV']);
disp(['Overpotential for H2 desorption: ', num2str(overpotential_H2), ' eV']);
```

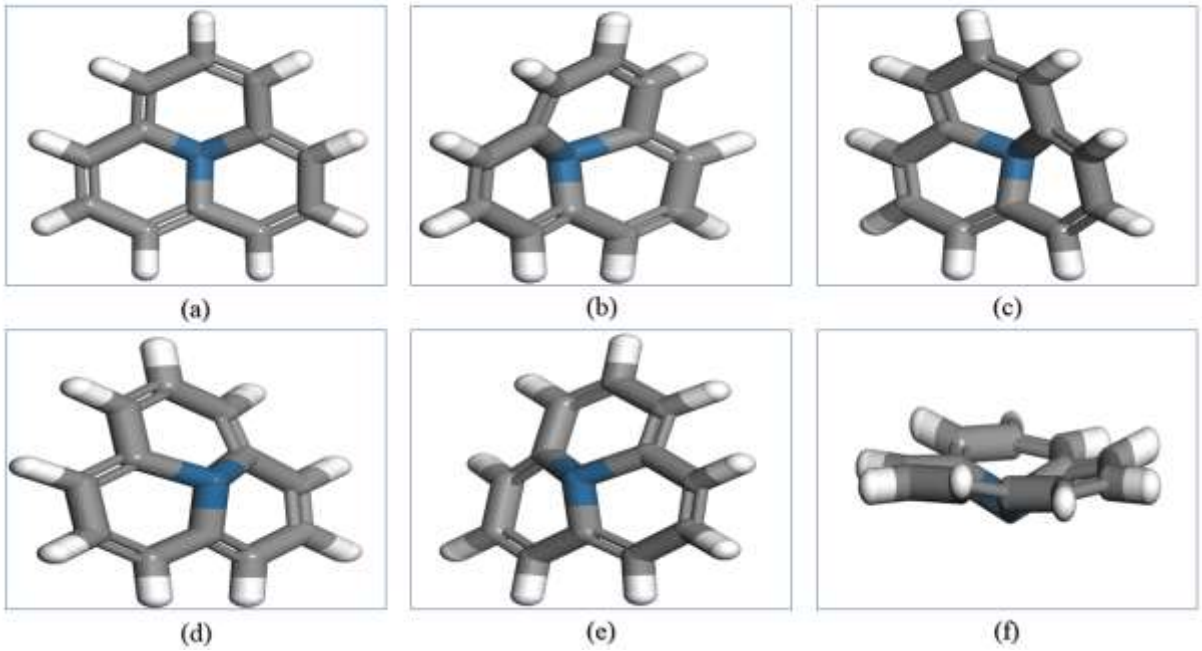


Figure 1: Pt-doped graphene basket (a-f)

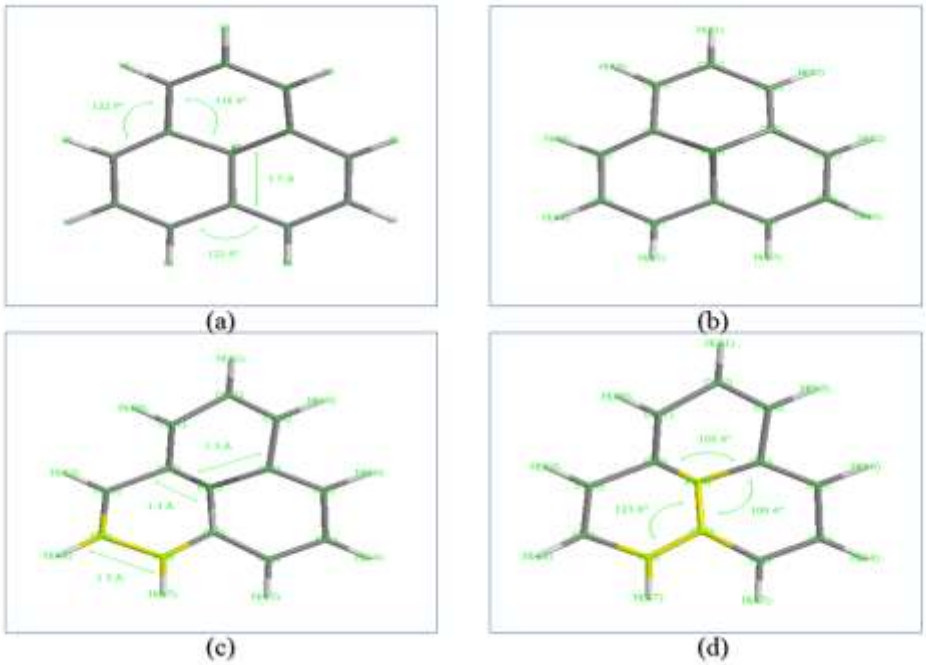


Figure 2: Structural Analysis of Phenalene (a) Bond length and bond angle of free phenalene (b) Atomic linkage of free (c) Bond length of Pt-doped Phenalene (d) Bond angle of the Pt-doped Phenalene

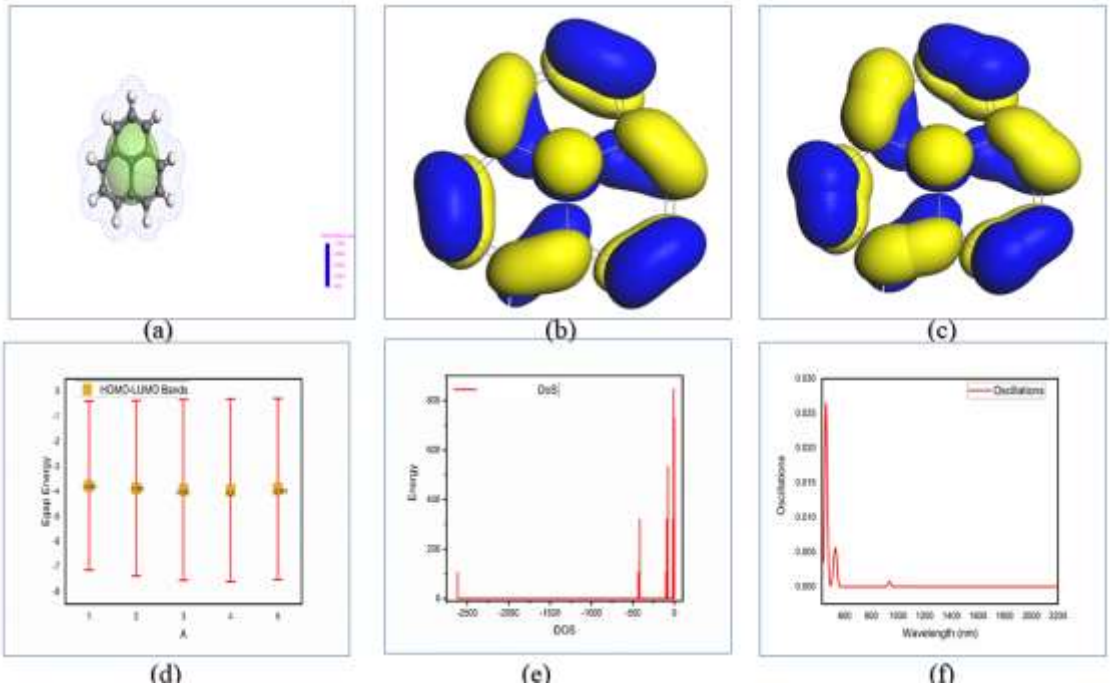


Figure 3: Electronic and optical Properties of Pt-Phenalene (a) Electron density (b) Highest Occupied Molecular Orbital of Pt-Doped Phenalene (c) Lowest Unoccupied Molecular Orbital of Pt-Doped Phenalene (d) HOMO-LUMO profile of PT-Doped Phenalene (e) Pt-Doped Phenalene DOS (f) Absorption spectrum of Pt-Doped Spectrum

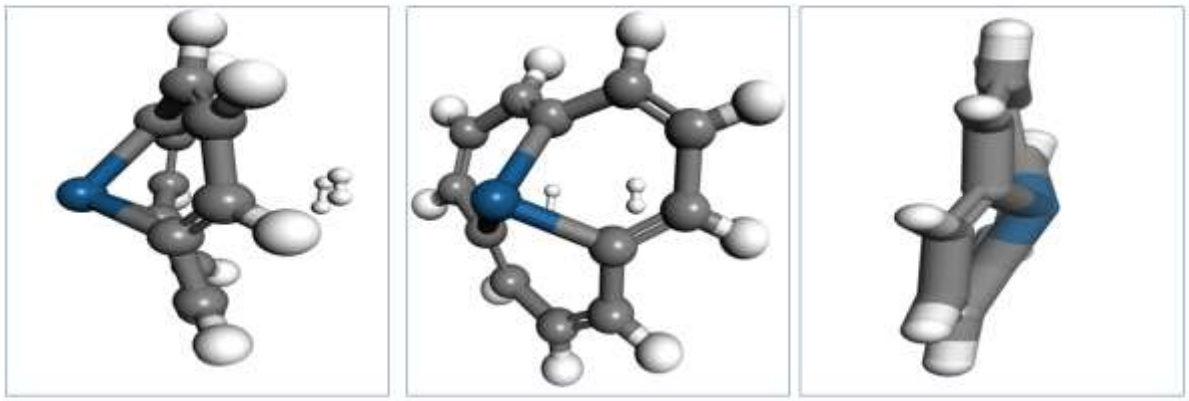


Figure 4: Adsorption orientation (a) Lateral Orientation of the adsorption Electrostatics (b) Anterior Orientation of the adsorption Electrostatics (c) Free Pt-doped phenalene Basket

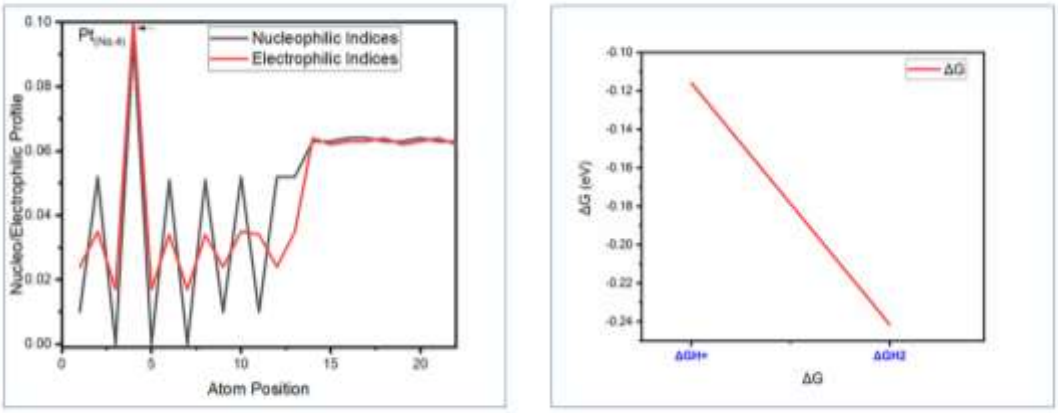


Figure 5: Fukui Profile for Pt-doped Phenalene (b) Tafel slope of Pt-Doped Phenalene

# 4.0 Result and Discussion

## 4.1 Structural Properties

The prevalent electrostatic properties of the model presents it as a catalytic basket due to the strong electronic character of platinum and how it behaves towards ensuring the aromaticity of the system is maintained. The structure (**Figure** 1) was confirmed to contain platinum, as evidenced by the reassignment of bond characteristics previously observed between **$C_4$-$C_5$**, **$C_5$-$C_6$**, and **$C_5$-$C_{10}$**. These bonds (**Table 1 and 2**) were redefined to reflect interactions involving platinum, specifically **$Pt_4$-$C_5$**, **$Pt_4$-$C_7$**, and **$Pt_4$-$C_3$**. This reassignment highlights the pivotal role of platinum in the structural configuration and bonding dynamics of the system.

The bond angles **$Pt_4$-$C_3$-$C_2$** (120.625°) and **$Pt_4$-$C_5$-$C_{10}$** (120.624°), which were absent in the pristine phenalene structure, are now present in the **Pt-doped phenalene**. These newly formed bond angles indicate the significant influence of platinum doping on the molecular geometry, altering the bond network and introducing new structural features not observed in the undoped system [61, 62].

## 4.2 Optical Properties

*Absorption Spectra:* The prominent peak at 0.233 (**Figure 3f**) oscillation evident in the (440-500)nm wavelength range underscores the substantial chromophoric activity of platinum-doped phenalene, attributable to robust π-π* and metal-to-ligand charge transfer (MLCT) transitions. This resonance indicates that platinum dopants considerably augment the light-harvesting capabilities of the phenalene system, thereby optimizing its interaction with visible light. The introduction of platinum into the molecular framework is likely to strengthen localized surface plasmon resonance (LSPR) effects, thereby amplifying the material's ability to generate photoinduced charge carriers. This property is critical for photophysical applications, as the strong

absorption in this range underpins its utility in catalytic systems, particularly in hydrogen evolution reactions (HER).

In contrast, the weak oscillation of 0.001 observed in the near-infrared (980 nm to 1000 nm) range indicates a subtle but measurable interaction with lower-energy photons, which may arise from extended vibrational overtones or weak long-wavelength resonance effects introduced by the platinum doping. While not as visible, the interaction in this spectral range could still contribute to catalytic activity. Such resonance could support electronic communication within the system, albeit indirectly. The combined optical features of platinum-doped phenalene impact charge recombination dynamics and HER efficiency. The strong visible light absorption ensures the generation of abundant charge carriers, while the presence of platinum facilitates rapid charge separation via its catalytic active sites, thereby minimizing charge recombination and enhancing the material's quantum efficiency. This ensures that the majority of the photogenerated electrons are utilized in the HER pathway.

The optical characteristics of platinum-doped phenalene impact charge separation, which is important for HER efficiency. The material's catalytic platinum active sites enable rapid separation of charge pairs and minimize charge recombination, increasing the quantum efficiency of the material. The photogenerated electrons are primarily used in the HER process due to this enhanced efficiency. Consequently, the material's tailored optical and electronic properties position it as a highly efficient photocatalyst for sustainable hydrogen production.

*HOMO-LUMO:* The HOMO-LUMO energy difference (**Table 3**) for platinum-doped phenalene (**Figure 3d)**, ranging from **-0.409 eV** to **-0.285 eV**, signifies a remarkably narrow electronic band gap, which has profound implications for its optical and optoelectronic properties [63]. This small gap suggests the material exhibits quasi-metallic behavior, facilitating low-energy electronic transitions and enhancing absorption in the near-infrared to visible spectral regions, making it highly suitable for photonic applications such as photodetectors and solar harvesting. Additionally, the reduced energy gap increases the polarizability of the system, potentially amplifying its nonlinear optical (**NLO**) responses, which are crucial for frequency conversion and all-optical switching. Furthermore, the ease of electronic excitation and charge transfer implied by this narrow gap could bolster the material's plasmonic behavior, enhancing localized surface plasmon resonance (**LSPR**) effects desirable in sensing and catalytic applications. The doping of phenalene with platinum not only narrows the band gap but also introduces tunability, allowing for precision tailoring of its optical absorption and emission profiles. Collectively, these properties make platinum-doped pyrene a promising candidate for advanced optical and optoelectronic applications.

## 4.3 Electronic Properties

*Electron Distribution:* The electron density distribution of Pt-doped phenalene (**Figure 3a**) reveals the strategic exposure of platinum within the molecular framework. The design aimed at optimizing the configuration where platinum atoms are situated at accessible sites. This placement ensures minimal steric hindrance and maximum interaction with the surrounding environment. Additionally, the electronic structure of the material may facilitate charge delocalization by caging the reactant, further enhancing the accessibility of platinum for chemical interactions. Such

structural and electronic attributes ensure that the platinum center is accessible within the matrix and are effectively presented for catalytic and electrochemical engagement.

This strategic exposure of platinum significantly enhances the catalytic photoelectrochemical performance of the material. The accessible platinum centers facilitate efficient electron transfer and adsorption of reactant molecules, critical for catalytic reactions like hydrogen evolution or other redox processes. The improved electron density near the platinum sites minimizes overpotentials, thereby increasing the catalytic efficiency and selectivity. Furthermore, the enhanced exposure reduces mass transport limitations, allowing reactants to interact with the active sites more readily. Collectively, this design not only boosts the catalytic activity but also improves the durability and reusability of the material in photoelectrochemical applications, making it a highly efficient and sustainable catalyst.

*Density of State:* The density of states (DOS) analysis for Pt-doped pyrene (**Figure 3e**), showing a cluster of high bands around the Fermi level, signifies a material with enhanced electronic density near the Fermi energy. This feature suggests a quasi-metallic or semi-metallic nature, characterized by a high density of electronic states available for conduction at minimal energy input [64]. The clustering of bands around the Fermi region implies delocalized electronic states, which facilitate efficient charge carrier transport and improved electrical conductivity.

Such a band structure is indicative of strong electronic interactions and overlapping energy levels, likely arising from the synergy between the platinum dopants and the phenalene matrix. The proximity of these bands to the Fermi level also enables facile electron excitation, contributing to the material's exceptional electrochemical and catalytic properties. This electronic architecture positions the material as an ideal candidate for applications requiring high charge mobility and robust electronic interactions, such as in advanced energy storage systems, electrocatalysis, and optoelectronics.

## 4.4 Adsorption Properties

*Mulliken Electrophilc Indices:* The Mulliken electrophilic indices (Figure 5a) reveal that platinum in the Pt-doped phenalene (Table 4) carries a partial positive charge of 0.101, whereas the bonding carbons ($C_3$, $C_5$, and $C_7$) have much smaller partial charges of 0.017. This charge disparity plays a crucial role in enhancing the catalytic efficiency of the system. The relatively higher positive charge on platinum indicates that it acts as a strong electrophile, effectively attracting electron density from the nearby carbons. This promotes the activation of adsorbed hydrogen atoms during the HER, facilitating efficient proton reduction. The electron density withdrawal from the carbon atoms makes them slightly more nucleophilic, creating a synergistic interaction with platinum, which enhances the overall catalytic activity by lowering the energy barrier for hydrogen desorption. This electrostatic configuration significantly improves the catalyst's performance, allowing for a lower overpotential and higher current densities in HER.

Regarding electron recombination, the charge distribution in the Pt-doped phenalene also plays a pivotal role in minimizing this detrimental effect. The higher positive charge on platinum creates an electron-deficient site that promotes charge separation upon excitation. This strong electrophilic character encourages the effective transfer of electrons from the adsorbate to the platinum center,

reducing the likelihood of charge pair recombination. The bonding carbons ($C_3$, $C_5$, and $C_7$), with their smaller partial charges, act as electron-rich centers that stabilize the electron density during the reaction. This stabilization, combined with the electrostatic interaction between the platinum and carbon atoms, prevents the recombination of electrons and holes, thereby enhancing the charge carrier lifetime. As a result, the Pt-doped phenalene maintains efficient electron flow, which is crucial for sustaining high catalytic activity and achieving long-term stability in electrochemical applications.

*Gibbs free Energy:* The observed Gibbs free energy values for $H_2$ (**-0.24157 eV**) and $H^+$ **(-0.11589 eV**) highlight the thermodynamic landscape of Pt-doped phenalene for HER. A material's efficiency for HER is significantly influenced by its ability to mediate proton adsorption, electron transfer, and molecular hydrogen desorption with minimal energy barriers. The relatively low Gibbs free energy for $H^+$ suggests that the material facilitates favorable adsorption of protons, an essential initial step in HER. Concurrently, the negative Gibbs free energy for $H_2$ indicates efficient desorption dynamics, crucial for sustaining catalytic turnover and preventing active site saturation.

The moderate disparity between the free energy values for $H^+$ and $H_2$ reflects a balanced adsorption-desorption process, a hallmark of an efficient HER catalyst. This balance minimizes the overpotential required for the reaction, enhancing the thermodynamic efficiency of hydrogen evolution. The synergy between the platinum dopant and the phenalene matrix likely optimizes the electronic structure and active site distribution, ensuring that the Gibbs free energy aligns closely with the thermoneutral value (ideal $\Delta G \approx 0$ eV) for hydrogen adsorption. These properties underscore the material's promise as a highly effective electrocatalyst for hydrogen evolution, combining favorable thermodynamics with robust catalytic activity.

*Tafel, Butler-Volmer Overpotential Indices:*

In this study we adopted the formula according to equation (5) to calculate the HER overpotential ($\eta$):

$$\eta = \Delta G_{act} - \Delta G_{thermoneutral} \qquad (5)$$

Where
$\eta$ is the overpotential, which represents the additional energy required for the reaction to occur beyond the ideal thermoneutral condition.
$\Delta G_{act}$ is the Gibbs free energy for the actual step in the HER process (either proton adsorption or hydrogen molecule desorption).
$\Delta G_{thermoneutral}$ is the Gibbs free energy at the thermoneutral point.

The overpotential essentially quantifies the energy barrier that must be overcome to drive the HER, with lower overpotentials indicating more efficient catalysis.

The calculated overpotentials for the HER based on the Gibbs free energies of **-0.11589 eV** for $H^+$ and **-0.24157 eV** for $H_2$ provide critical insight into the electrocatalytic efficiency of the Pt-doped phenalene material (**Figure 5b)**. The overpotentials for both proton adsorption and hydrogen desorption are relatively low, suggesting that the material facilitates favorable proton adsorption

at its surface and efficient hydrogen molecule desorption. A low overpotential is crucial because it indicates minimal energy losses during the HER process, thereby enhancing the overall efficiency of the reaction. Specifically, the moderate overpotentials reflect a balanced adsorption-desorption mechanism, reducing the need for excessive energy input and optimizing the catalytic activity. These properties align closely with ideal HER performance, where the Gibbs free energies approach the thermoneutral value (0 eV), minimizing overpotentials. As such, Pt-doped pyrene demonstrates considerable promise as an efficient electrocatalyst for HER, capable of achieving high catalytic turnover with lower energy consumption, making it a potential candidate for sustainable hydrogen production in electrochemical energy conversion systems.

**Table 1: Structural Properties of Phenalene**

| | Bond Angle | | | Bond Length | |
|---|---|---|---|---|---|
| **Atoms** | **Actual (° / Å)** | **Optimal (° / Å)** | **Atoms** | **Actual (° / Å)** | **Optimal (° / Å)** |
| H(23)-C(13)-C(6) | 119.66 | 120 | C(13)-H(23) | 1.1 | 1.1 |
| H(23)-C(13)-C(12) | 119.66 | 120 | C(12)-H(22) | 1.1 | 1.1 |
| C(6)-C(13)-C(12) | 120.681 | | C(11)-H(21) | 1.1 | 1.1 |
| H(22)-C(12)-C(13) | 119.046 | 120 | C(9)-H(20) | 1.1 | 1.1 |
| H(22)-C(12)-C(1) | 119.046 | 120 | C(8)-H(19) | 1.1 | 1.1 |
| C(13)-C(12)-C(1) | 121.908 | | C(7)-H(18) | 1.1 | 1.1 |
| H(21)-C(11)-C(6) | 119.434 | 120 | C(5)-H(17) | 1.113 | 1.113 |
| H(21)-C(11)-C(2) | 119.434 | 120 | C(3)-H(16) | 1.1 | 1.1 |
| C(6)-C(11)-C(2) | 121.133 | | C(2)-H(15) | 1.1 | 1.1 |
| C(1)-C(10)-C(5) | 116.551 | 121.4 | C(1)-H(14) | 1.1 | 1.1 |
| C(1)-C(10)-C(9) | 122.938 | 120 | C(6)-C(13) | 1.345 | 1.337 |
| C(5)-C(10)-C(9) | 120.509 | 121.4 | C(12)-C(13) | 1.45 | 1.503 |
| H(20)-C(9)-C(10) | 119.658 | 120 | C(1)-C(12) | 1.343 | 1.337 |
| H(20)-C(9)-C(8) | 119.658 | 120 | C(10)-C(1) | 1.454 | 1.503 |
| C(10)-C(9)-C(8) | 120.685 | | C(5)-C(10) | 1.53 | 1.497 |
| H(19)-C(8)-C(9) | 119.044 | 120 | C(9)-C(10) | 1.345 | 1.337 |
| H(19)-C(8)-C(7) | 119.044 | 120 | C(8)-C(9) | 1.45 | 1.503 |
| C(9)-C(8)-C(7) | 121.911 | | C(7)-C(8) | 1.343 | 1.337 |
| H(18)-C(7)-C(8) | 119.436 | 120 | C(4)-C(7) | 1.454 | 1.503 |
| H(18)-C(7)-C(4) | 119.436 | 120 | C(11)-C(6) | 1.454 | 1.503 |
| C(8)-C(7)-C(4) | 121.129 | | C(5)-C(6) | 1.53 | 1.497 |
| C(13)-C(6)-C(11) | 122.931 | 120 | C(4)-C(5) | 1.53 | 1.497 |
| C(13)-C(6)-C(5) | 120.518 | 121.4 | C(3)-C(4) | 1.345 | 1.337 |
| C(11)-C(6)-C(5) | 116.55 | 121.4 | C(2)-C(3) | 1.449 | 1.503 |

| | | | | | |
|---|---|---|---|---|---|
| H(17)-C(5)-C(10) | 105.814 | 109.39 | C(11)-C(2) | 1.343 | 1.337 |
| H(17)-C(5)-C(6) | 105.809 | 109.39 | | | |
| H(17)-C(5)-C(4) | 105.804 | 109.39 | | | |
| C(10)-C(5)-C(6) | 112.868 | 109.51 | | | |
| C(10)-C(5)-C(4) | 112.872 | 109.51 | | | |
| C(6)-C(5)-C(4) | 112.876 | 109.51 | | | |
| C(7)-C(4)-C(5) | 116.557 | 121.4 | | | |
| C(7)-C(4)-C(3) | 122.929 | 120 | | | |
| C(5)-C(4)-C(3) | 120.513 | 121.4 | | | |
| H(16)-C(3)-C(4) | 119.66 | 120 | | | |
| H(16)-C(3)-C(2) | 119.66 | 120 | | | |
| C(4)-C(3)-C(2) | 120.68 | | | | |
| H(15)-C(2)-C(3) | 119.045 | 120 | | | |
| H(15)-C(2)-C(11) | 119.045 | 120 | | | |
| C(3)-C(2)-C(11) | 121.911 | | | | |
| H(14)-C(1)-C(12) | 119.432 | 120 | | | |
| H(14)-C(1)-C(10) | 119.432 | 120 | | | |
| C(12)-C(1)-C(10) | 121.135 | | | | |

**Table 1: Structural Properties of Platinum-doped Phenalene**

| Bond Length | | | Bond Angle | | |
|---|---|---|---|---|---|
| **Atoms** | **Actual (° / Å)** | **Optimal (° / Å)** | **Atom** | **Actual (° / Å)** | **Optimal (° / Å)** |
| C(13)-H(22) | 1.1 | 1.1 | H(22)-C(13)-C(9) | 116.93 | 120 |
| C(12)-H(21) | 1.1 | 1.1 | H(22)-C(13)-C(7) | 122.99 | 120 |
| C(11)-H(20) | 1.1 | 1.1 | C(9)-C(13)-C(7) | 119.854 | |
| C(12)-C(11) | 1.45 | 1.503 | H(21)-C(12)-C(11) | 123.835 | 120 |
| C(10)-H(19) | 1.1 | 1.1 | H(21)-C(12)-C(10) | 124.465 | 120 |
| C(10)-C(12) | 1.343 | 1.337 | C(11)-C(12)-C(10) | 111.495 | |
| C(9)-H(18) | 1.1 | 1.1 | H(20)-C(11)-C(12) | 114.491 | 120 |
| C(13)-C(9) | 1.343 | 1.337 | H(20)-C(11)-C(7) | 123.148 | 120 |
| C(8)-H(17) | 1.1 | 1.1 | C(12)-C(11)-C(7) | 122.356 | |
| C(9)-C(8) | 1.449 | 1.503 | H(19)-C(10)-C(12) | 116.93 | 120 |
| C(13)-C(7) | 1.454 | 1.503 | H(19)-C(10)-C(5) | 122.99 | 120 |
| C(7)-C(11) | 1.345 | 1.337 | C(12)-C(10)-C(5) | 119.854 | |
| C(6)-H(16) | 1.1 | 1.1 | H(18)-C(9)-C(13) | 124.465 | 120 |
| C(5)-C(10) | 1.454 | 1.503 | H(18)-C(9)-C(8) | 123.835 | 120 |
| C(6)-C(5) | 1.345 | 1.337 | C(13)-C(9)-C(8) | 111.495 | |
| Pt(4)-C(7) | 1.53 | 1.346 | H(17)-C(8)-C(9) | 114.49 | 120 |
| Pt(4)-C(5) | 1.53 | 1.346 | H(17)-C(8)-C(3) | 123.148 | 120 |
| C(8)-C(3) | 1.345 | 1.337 | C(9)-C(8)-C(3) | 122.356 | |
| C(3)-Pt(4) | 1.53 | 1.346 | C(13)-C(7)-C(11) | 113.965 | 120 |
| C(2)-H(15) | 1.1 | 1.1 | C(13)-C(7)-Pt(4) | 120.624 | |
| C(3)-C(2) | 1.454 | 1.503 | C(11)-C(7)-Pt(4) | 123.555 | |
| C(1)-H(14) | 1.1 | 1.1 | H(16)-C(6)-C(5) | 123.148 | 120 |
| C(1)-C(6) | 1.45 | 1.503 | H(16)-C(6)-C(1) | 114.49 | 120 |
| C(2)-C(1) | 1.343 | 1.337 | C(5)-C(6)-C(1) | 122.357 | |
| | | | C(10)-C(5)-C(6) | 113.967 | 120 |
| | | | C(10)-C(5)-Pt(4) | 120.624 | |
| | | | C(6)-C(5)-Pt(4) | 123.554 | |
| | | | C(7)-Pt(4)-C(5) | 109.429 | |
| | | | C(7)-Pt(4)-C(3) | 109.429 | |
| | | | C(5)-Pt(4)-C(3) | 109.43 | |
| | | | C(8)-C(3)-Pt(4) | 123.554 | |
| | | | C(8)-C(3)-C(2) | 113.965 | 120 |
| | | | Pt(4)-C(3)-C(2) | 120.625 | |
| | | | H(15)-C(2)-C(3) | 122.989 | 120 |
| | | | H(15)-C(2)-C(1) | 116.931 | 120 |
| | | | C(3)-C(2)-C(1) | 119.853 | |
| | | | H(14)-C(1)-C(6) | 123.835 | 120 |
| | | | H(14)-C(1)-C(2) | 124.464 | 120 |

| | | |
|---|---|---|
| C(6)-C(1)-C(2) | 111.496 | |

**Table 3: HOMO-LUMO Characters of Pt-doped Phenalene**

| | Egap Energy | LUMO | Egap Energy |
|---|---|---|---|
| 1 | -3.776 | -3.367 | -0.409 |
| 2 | -3.875 | -3.507 | -0.368 |
| 3 | -3.936 | -3.605 | -0.331 |
| 4 | -3.951 | -3.651 | -0.3 |
| 5 | -3.903 | -3.618 | -0.285 |
| 6 | -3.802 | -3.513 | -0.289 |
| 7 | -3.72 | -3.415 | -0.305 |
| 8 | -3.702 | -3.393 | -0.309 |
| 9 | -3.686 | -3.372 | -0.314 |
| 10 | -3.686 | -3.369 | -0.317 |
| 11 | -3.687 | -3.37 | -0.317 |

Table 4: Mulliken Fukui Characters

| | Mulliken Fukui Indices | |
|---|---|---|
| **Atom** | **Neucleophilic Indices** | **Electrophilic Indices** |
| 1 | 0.01 | 0.024 |
| 2 | 0.052 | 0.035 |
| 3 | 0 | 0.017 |
| 4 | 0.095 | 0.101 |
| 5 | 0 | 0.017 |
| 6 | 0.051 | 0.034 |
| 7 | 0 | 0.017 |
| 8 | 0.051 | 0.034 |
| 9 | 0.01 | 0.024 |
| 10 | 0.052 | 0.035 |
| 11 | 0.01 | 0.034 |
| 12 | 0.052 | 0.024 |
| 13 | 0.052 | 0.035 |
| 14 | 0.063 | 0.064 |
| 15 | 0.063 | 0.062 |
| 16 | 0.064 | 0.063 |
| 17 | 0.064 | 0.063 |
| 18 | 0.063 | 0.064 |
| 19 | 0.063 | 0.062 |
| 20 | 0.064 | 0.063 |

| | | |
|---|---|---|
| 21 | 0.063 | 0.064 |
| 22 | 0.063 | 0.062 |

## 5.0 Conclusion

In conclusion, the model demonstrated a comparable Gibbs free energy and overpotential, indicating its potential for efficient catalytic performance. The electron density analysis revealed significant and effective charge redistribution, further supporting the enhanced reactivity of the system. Additionally, the Fukui indices confirmed that the model exhibits a stable and ideal electronic profile, capable of minimizing electron recombination, which is crucial for maintaining high catalytic efficiency over extended periods. The presence of multiple optical absorption peaks and a favorable HOMO-LUMO gap underscores the material's suitability for photocatalytic applications, where effective charge separation and light absorption are key to promoting efficient photocatalysis.

Moreover, the strategically positioned adsorption bands within the visible and near-infrared ranges place the model as an ideal solution to the persistent challenge of charge recombination, ensuring superior carrier dynamics and sustained reactivity. These spectral features not only enhance light-harvesting efficiency but also open avenues for overcoming limitations in current catalytic designs, thereby setting the stage for breakthroughs in scaling hydrogen evolution technologies.

Collectively, these findings highlight the Pt-doped phenalene model's promising performance as a highly efficient and stable catalyst. Its tailored optical and electronic properties make it a strong candidate for advancing photocatalytic energy conversion and environmental remediation processes, pushing the boundaries of sustainable hydrogen production.

## 6.0 References


1. He, Y., Zhang, Y., Hao, G., Jiang, W., & Di, J. (2024). Single atoms meeting 2D materials: an excellent configuration for photocatalysis. *Nanoscale*, *16*(48), 22077-22098.
2. Gao, C., Low, J., Long, R., Kong, T., Zhu, J., & Xiong, Y. (2020). Heterogeneous single-atom photocatalysts: fundamentals and applications. *Chemical reviews*, *120*(21), 12175-12216.
3. Wei, T., Zhou, J., & An, X. (2024). Recent advances in single-atom catalysts (SACs) for photocatalytic applications. *Materials Reports: Energy*, 100285.
4. Guo, Y., Zhou, Q., Zhu, B., Tang, C. Y., & Zhu, Y. (2023). Advances in organic semiconductors for photocatalytic hydrogen evolution reaction. *EES Catalysis*, *1*(4), 333-352.
5. Kosco, J., Moruzzi, F., Willner, B., & McCulloch, I. (2020). Photocatalysts based on organic semiconductors with tunable energy levels for solar fuel applications. *Advanced Energy Materials*, *10*(39), 2001935.
6. Dai, C., & Liu, B. (2020). Conjugated polymers for visible-light-driven photocatalysis. *Energy & Environmental Science*, *13*(1), 24-52.
7. Chen, Y., Yan, C., Dong, J., Zhou, W., Rosei, F., Feng, Y., & Wang, L. N. (2021). Structure/property control in photocatalytic organic semiconductor nanocrystals. *Advanced Functional Materials*, *31*(36), 2104099.
8. Dong, J., Yan, C., Chen, Y., Zhou, W., Peng, Y., Zhang, Y., ... & Huang, Z. H. (2022). Organic semiconductor nanostructures: Optoelectronic properties, modification strategies, and photocatalytic applications. *Journal of Materials Science & Technology*, *113*, 175-198.
9. Marin, M. L., Santos-Juanes, L., Arques, A., Amat, A. M., & Miranda, M. A. (2012). Organic photocatalysts for the oxidation of pollutants and model compounds. *Chemical reviews*, *112*(3), 1710-1750.
10. Khan, K., Rehman, Z. U., Yao, S., Bajpai, O. P., Miotello, A., Nawaz, M., ... & Zaki, M. E. (2024). Nanoscale engineering of semiconductor photocatalysts boosting charge separation for solar-driven H2 production: Recent advances and future perspective. *Nanotechnology Reviews*, *13*(1), 20240104.
11. Rahman, M. Z., Kibria, M. G., & Mullins, C. B. (2020). Metal-free photocatalysts for hydrogen evolution. *Chemical Society Reviews*, *49*(6), 1887-1931.
12. Rahman, M., Tian, H., & Edvinsson, T. (2020). Revisiting the limiting factors for overall water-splitting on organic photocatalysts. *Angewandte Chemie*, *132*(38), 16418-16433.
13. Abhishek, B., Jayarama, A., Rao, A. S., Nagarkar, S. S., Dutta, A., Duttagupta, S. P., ... & Pinto, R. (2024). Challenges in photocatalytic hydrogen evolution: Importance of photocatalysts and photocatalytic reactors. *International Journal of Hydrogen Energy*, *81*, 1442-1466.
14. Guo, Y., Zhou, Q., Zhu, B., Tang, C. Y., & Zhu, Y. (2023). Advances in organic semiconductors for photocatalytic hydrogen evolution reaction. *EES Catalysis*, *1*(4), 333-352.
15. Qiu, X., Zhang, Y., Zhu, Y., Long, C., Su, L., Liu, S., & Tang, Z. (2021). Applications of nanomaterials in asymmetric photocatalysis: recent progress, challenges, and opportunities. *Advanced Materials*, *33*(6), 2001731.
16. Xiong, L., & Tang, J. (2021). Strategies and challenges on selectivity of photocatalytic oxidation of organic substances. *Advanced Energy Materials*, *11*(8), 2003216.
17. Fang, X., Choi, J. Y., Stodolka, M., Pham, H. T., & Park, J. (2024). Advancing Electrically Conductive Metal–Organic Frameworks for Photocatalytic Energy Conversion. *Accounts of Chemical Research*, *57*(16), 2316-2325.
18. Rahman, M. Z., & Mullins, C. B. (2018). Understanding charge transport in carbon nitride for enhanced photocatalytic solar fuel production. *Accounts of chemical research*, *52*(1), 248-257.
19. Chen, F., Ma, T., Zhang, T., Zhang, Y., & Huang, H. (2021). Atomic-level charge separation strategies in semiconductor-based photocatalysts. *Advanced Materials*, *33*(10), 2005256.
20. Rappaport, F., Guergova-Kuras, M., Nixon, P. J., Diner, B. A., & Lavergne, J. (2002). Kinetics and pathways of charge recombination in photosystem II. *Biochemistry*, *41*(26), 8518-8527.

21. Wu, Y., Chen, Y., Li, D., Sajjad, D., Chen, Y., Sun, Y., ... & Jiang, Z. (2022). Interface engineering of organic-inorganic heterojunctions with enhanced charge transfer. *Applied Catalysis B: Environmental*, *309*, 121261.
22. Kosco, J., Moruzzi, F., Willner, B., & McCulloch, I. (2020). Photocatalysts based on organic semiconductors with tunable energy levels for solar fuel applications. *Advanced Energy Materials*, *10*(39), 2001935.
23. Wang, Q., & Domen, K. (2019). Particulate photocatalysts for light-driven water splitting: mechanisms, challenges, and design strategies. *Chemical Reviews*, *120*(2), 919-985.
24. Ferrão, L. F., Pontes, M. A., Fernandes, G. F., Bettanin, F., Aquino, A. J., Lischka, H., ... & Machado, F. B. (2023). Stability and Reactivity of the Phenalene and Olympicene Isomers. *The Journal of Physical Chemistry A*, *127*(45), 9430-9441.
25. Biagiotti, G., Perini, I., Richichi, B., & Cicchi, S. (2021). Novel Synthetic Approach to Heteroatom Doped Polycyclic Aromatic Hydrocarbons: Optimizing the Bottom-Up Approach to Atomically Precise Doped Nanographenes. *Molecules*, *26*(20), 6306.
26. Hurmalainen, J. (2017). *Experimental and computational studies of unconventional main group compounds: stable radicals and reactive intermediates* (Doctoral dissertation, University of Jyväskylä).
27. Morita, Y., & Nishida, S. (2010). Phenalenyls, cyclopentadienyls, and other carbon-centered radicals. *Stable radicals: fundamentals and applied aspects of odd-electron Compounds*, 81-145.
28. Ahmed, J., & Mandal, S. K. (2022). Phenalenyl radical: Smallest polycyclic odd alternant hydrocarbon present in the graphene sheet. *Chemical Reviews*, *122*(13), 11369-11431.
29. Poater, J., Duran, M., & Solà, M. (2018). Aromaticity determines the relative stability of kinked vs. straight topologies in polycyclic aromatic hydrocarbons. *Frontiers in chemistry*, *6*, 425890.
30. Uchida, K., & Kubo, T. (2016). Recent advances in the chemistry of phenalenyl. *Journal of Synthetic Organic Chemistry, Japan*, *74*(11), 1069-1077.
31. Stepien, M., Gonka, E., Żyła, M., & Sprutta, N. (2017). Heterocyclic nanographenes and other polycyclic heteroaromatic compounds: synthetic routes, properties, and applications. *Chemical reviews*, *117*(4), 3479-3716.
32. Ahmed, J., & Mandal, S. K. (2022). Phenalenyl radical: Smallest polycyclic odd alternant hydrocarbon present in the graphene sheet. *Chemical Reviews*, *122*(13), 11369-11431.
33. Ahmed, J., & Mandal, S. K. (2022). Phenalenyl radical: Smallest polycyclic odd alternant hydrocarbon present in the graphene sheet. *Chemical Reviews*, *122*(13), 11369-11431.
34. Wu, J., Pisula, W., & Müllen, K. (2007). Graphenes as potential material for electronics. *Chemical reviews*, *107*(3), 718-747.
35. Fatima, S., Muhammad, S., Bibi, S., Munawar, K. S., Al-Sehemi, A. G., Chaudhry, A. R., & Adnan, M. (2024). Quantum chemical framework for tailoring N/B doped phenalene derivatives to achieve high performance nonlinear optical materials. *Journal of Molecular Graphics and Modelling*, *128*, 108723.
36. Huang, W. (1990). *The approaches to 13-methylphenalene system and the studies of aromaticity and antiaromaticity*. City University of New York.
37. Fei, Y., & Liu, J. (2022). Synthesis of defective nanographenes containing joined pentagons and heptagons. *Advanced Science*, *9*(19), 2201000.
38. Manjavacas, A., Marchesin, F., Thongrattanasiri, S., Koval, P., Nordlander, P., Sánchez-Portal, D., & García de Abajo, F. J. (2013). Tunable molecular plasmons in polycyclic aromatic hydrocarbons. *ACS nano*, *7*(4), 3635-3643.
39. Deng, C. L., Hollister, K. K., Molino, A., Tra, B. Y. E., Dickie, D. A., Wilson, D. J., & Gilliard Jr, R. J. (2024). Unveiling Three Interconvertible Redox States of Boraphenalene. *Journal of the American Chemical Society*, *146*(9), 6145-6156.

40. Biagiotti, G., Perini, I., Richichi, B., & Cicchi, S. (2021). Novel Synthetic Approach to Heteroatom Doped Polycyclic Aromatic Hydrocarbons: Optimizing the Bottom-Up Approach to Atomically Precise Doped Nanographenes. *Molecules*, *26*(20), 6306.
41. Ahmed, J., & Mandal, S. K. (2022). Phenalenyl radical: Smallest polycyclic odd alternant hydrocarbon present in the graphene sheet. *Chemical Reviews*, *122*(13), 11369-11431.
42. Levey, Z. (2022). *A Spectroscopic Investigation of the Phenalenyl Radical and its Formation* (Doctoral dissertation, UNSW Sydney).
43. Reid, D. H. (1965). The chemistry of the phenalenes. *Quarterly Reviews, Chemical Society*, *19*(3), 274-302.
44. Rieger, R., & Müllen, K. (2010). Forever young: polycyclic aromatic hydrocarbons as model cases for structural and optical studies. *Journal of Physical Organic Chemistry*, *23*(4), 315-325.
45. O'Brien, S. (1962). *The Synthesis and Properties of Some Heterocyclic Analogues of Phenalene*. The University of Manchester (United Kingdom).
46. Lu, H., Mack, J., Yang, Y., & Shen, Z. (2014). Structural modification strategies for the rational design of red/NIR region BODIPYs. *Chemical Society Reviews*, *43*(13), 4778-4823.
47. Anamimoghadam, O. (2013). *9-C-substituted phenalenones as promising precursors for the synthesis of novel stable phenalenyl-type cations and radicals* (Doctoral dissertation, University of Glasgow).
48. Chen, D. (2022). *Design and synthesis of blue thermally activated delayed fluorescence emitters for organic light emitting diodes* (Doctoral dissertation, University of St Andrews).
49. Deekamwong, K. Photoactive Hexaazaphenalene Ligand-based Frameworks and Their Applications.
50. Kemppainen, E., Bodin, A., Sebok, B., Pedersen, T., Seger, B., Mei, B., ... & Chorkendorff, I. (2015). Scalability and feasibility of photoelectrochemical H 2 evolution: the ultimate limit of Pt nanoparticle as an HER catalyst. *Energy & Environmental Science*, *8*(10), 2991-2999.
51. Cheng, N., Stambula, S., Wang, D., Banis, M. N., Liu, J., Riese, A., ... & Sun, X. (2016). Platinum single-atom and cluster catalysis of the hydrogen evolution reaction. *Nature communications*, *7*(1), 13638.
52. Chen, A., & Holt-Hindle, P. (2010). Platinum-based nanostructured materials: synthesis, properties, and applications. *Chemical reviews*, *110*(6), 3767-3804.
53. Ooka, H., Wintzer, M. E., & Nakamura, R. (2021). Non-zero binding enhances kinetics of catalysis: Machine learning analysis on the experimental hydrogen binding energy of platinum. *ACS Catalysis*, *11*(10), 6298-6303.
54. Zhou, K. L., Wang, Z., Han, C. B., Ke, X., Wang, C., Jin, Y., ... & Yan, H. (2021). Platinum single-atom catalyst coupled with transition metal/metal oxide heterostructure for accelerating alkaline hydrogen evolution reaction. *Nature Communications*, *12*(1), 3783.
55. Huang, Y., Quan, W., Yao, H., Yang, R., Hong, Z., & Lin, Y. (2023). Recent advances in surface reconstruction toward self-adaptive electrocatalysis: a review. *Inorganic Chemistry Frontiers*, *10*(2), 352-369.
56. Chatterjee, A., & Chatterjee, M. (2011). 2 Computational Designing of Gradient-Type Catalytic Membrane. *Industrial Applications of Molecular Simulations*, 23.
57. Zhuang, J., Tang, T., Ding, Y., Tatikonda, S. C., Dvornek, N., Papademetris, X., & Duncan, J. (2020). Adabelief optimizer: Adapting stepsizes by the belief in observed gradients. *Advances in neural information processing systems*, *33*, 18795-18806.
58. Song, L., Liu, W., Xin, F., & Li, Y. (2021). " Materials Studio" simulation study of the adsorption and polymerization mechanism of sodium silicate on active silica surface at different temperatures. *International Journal of Metalcasting*, *15*, 1091-1098.
59. Issa, A. A., Kamel, M. D., & El-Sayed, D. S. (2024). Depicted simulation model for removal of second-generation antipsychotic drugs adsorbed on Zn-MOF: adsorption locator assessment. *Journal of Molecular Modeling*, *30*(4), 106.

60. Halgren, T. A. (1992). The representation of van der Waals (vdW) interactions in molecular mechanics force fields: potential form, combination rules, and vdW parameters. *Journal of the American Chemical Society*, *114*(20), 7827-7843.
61. Groves, M. N., Malardier-Jugroot, C., & Jugroot, M. (2012). Improving platinum catalyst durability with a doped graphene support. *The Journal of Physical Chemistry C*, *116*(19), 10548-10556.
62. Meng, Z., Xia, T., Wang, Z., & Hu, X. (2024). Enhanced adsorption and sensing properties of Ptn (n= 1, 3)-doped SnS2 monolayers for warfare toxic gases: A DFT Study. *Sensors and Actuators A: Physical*, *380*, 116044.
63. Tang, L., Pan, X., Luo, M., Yang, R., Guo, L., Sun, Z., ... & Zhu, Q. (2023). Boosting ultrasensitive SERS activity on quasi-metallic tungsten oxide through synergistic vibronic coupling and electromagnetic resonance. *Journal of Materials Chemistry A*, *11*(30), 16212-16220.
64. Erben, D. (2020). *Optical and Electronic Properties of Atomically Thin Transition-Metal Dichalcogenides* (Doctoral dissertation, Universität Bremen).